ACS ES&T Water

pubs.acs.org/estwater

Article

Overlooked Combined Ecotoxicological Risk of Naturally Occurring Beryllium and Thallium in Sediments to Aquatic Biota: An SPI Model-Based Assessment in the Pearl River Estuary

Yang-Guang Gu,* Yan-Peng Gao, Rui-Ze Liang, Richard W. Jordan, and Shi-Jun Jiang

Cite This: *ACS EST Water* 2025, 5, 5145−5156

Read Online

ACCESS | Metrics & More | Article Recommendations | Supporting Information

ABSTRACT: Beryllium (Be) and thallium (Tl) are highly toxic, naturally occurring trace metals increasingly recognized as emerging contaminants in aquatic ecosystems. Sediments act as both a major sink and a potential source of these metals, influencing their bioavailability and ecological impact. However, their combined adverse biological effects on aquatic biota in natural sedimentary environments remain unknown. This study presents the first quantitative ecotoxicological risk assessment of Be and Tl in surface sediments using the SPI model, which integrates species sensitivity distribution, probabilistic risk assessment, and the inclusion-exclusion principle. Due to the lack of an established diffusive gradients in thin films protocol for Be and Tl, we employed a validated transformation model to convert weak acid-exchangeable sediment concentrations (mg/kg) into estimated aqueous-phase concentrations (mg/L). These were used as inputs for the SPI model. Sediment samples from the Pearl River Estuary showed a 37.05% probability of combined toxic effects, exceeding the 25% ecological risk threshold and indicating a mild ecotoxicological risk. This study introduces a novel framework for evaluating the bioavailability and joint risk of Be and Tl in sediments, providing new insights for estuarine ecological risk assessment and environmental policy development.

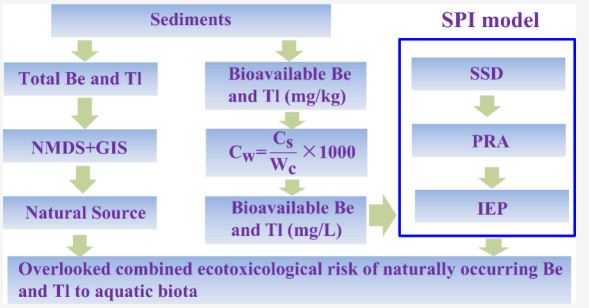

KEYWORDS: *emerging contaminants, trace metal toxicity, sediment bioavailability, combined ecological risk, probabilistic risk assessment, estuarine ecosystem health*

1. INTRODUCTION

Beryllium (Be) and thallium (Tl) have recently been recognized as emerging contaminants due to their high toxicity, environmental persistence, and potential risks to aquatic ecosystems.[1−6] Although both metals occur naturally, their presence in aquatic environments is increasingly influenced by anthropogenic activities such as mining, metallurgy, and industrial discharge.[1−5,7] Additionally, natural processes such as rock weathering, soil erosion, and volcanic activity contribute to their mobilization, influencing their geochemical cycling and bioavailability.[8−11] However, the ecotoxicological risks posed by naturally occurring Be and Tl have often been overlooked or misattributed solely to anthropogenic sources, leading to a potential underestimation of their environmental impact.

Sediments serve as both a major sink and source of contaminants in aquatic environments, playing a crucial role in the transport, transformation, and bioavailability of trace metals.[12−15] Be and Tl tend to accumulate in sediments, where they may persist for long periods and subsequently be remobilized into the water column under changing environmental conditions.[6,7,16,17] Despite the recognized role of sediments in metal biogeochemistry, there is a critical lack of research assessing the combined adverse effects of Be and Tl on aquatic biota in sediments, particularly in terms of their bioavailability and ecological impact. Unlike well-studied heavy metals such as lead (Pb), cadmium (Cd), and mercury (Hg),[13,18,19] the bioavailability and ecotoxicological effects of Be and Tl remain poorly understood, hindering the development of effective risk assessment frameworks and regulatory strategies.

Although previous studies have documented the occurrence of Be and Tl in various water bodies,[7,16,20−24] no prior research has quantitatively assessed their joint adverse effects on aquatic biota in natural ecosystems. Be is known for its carcinogenic properties, while Tl is extremely toxic to aquatic life, disrupting critical physiological processes even at low concentrations.[1,3,4,25−27] However, their environmental risks are often underestimated due to the lack of suitable bioavailability assessment methods. As a widely recognized tool for

Received: March 17, 2025
Revised: July 29, 2025
Accepted: July 30, 2025
Published: August 5, 2025

https://doi.org/10.1021/acsestwater.5c00307
ACS EST Water 2025, 5, 5145−5156

Figure 1. Map of the study area illustrating location of (A, B) Pearl River Estuary in China and (C) sampled sites in the Pearl River Estuary intertidal zone.

bioavailability assessment, diffusive gradients in thin films (DGT) technology provides in situ measurements of labile metal concentrations, offering a valuable approach for estimating their potential uptake by aquatic organisms.[13,14,28−30] However, no established DGT protocol exists for Be and Tl. To address this limitation, this study applies a validated transformation model to estimate their bioavailable fractions, converting weak acid-exchangeable sediment concentrations (mg/kg) into aqueous-phase concentrations (mg/L) (Section 2.3). This approach provides a practical alternative for assessing Be and Tl bioavailability in sediments, bridging the methodological gap in metal bioavailability quantification.

Furthermore, this study is the first to apply the SPI model (species sensitivity distribution−probabilistic risk assessment−inclusion-exclusion principle) to assess the ecological risk of Be and Tl. The SPI model offers a novel solution by integrating multiple risk assessment components, enabling a more precise evaluation of metal-induced ecological threats. Existing research predominantly evaluates the probabilistic ecotoxicological risks posed by individual contaminants or persistent organic pollutants to aquatic organisms.[31−34] However, there remains a significant gap in methodologies for quantitatively assessing the cumulative ecotoxicological risks arising from diverse pollutant categories, including inorganic contaminants, organic chemicals, and microplastics. To address this limitation, Gu et al.[33] developed the SPI model, which integrates SSD, PRA, and the IEP to systematically quantify the ecotoxicological risks of rare earth elements (REEs) to aquatic species. Since its inception, the SPI model has been adapted to evaluate the collective risks of various pollutants, providing a more holistic approach to quantitative ecotoxicological risk assessment.[13,33,35−37] Unlike traditional risk assess-

https://doi.org/10.1021/acsestwater.5c00307
ACS EST Water 2025, 5, 5145−5156

ment models that focus on single pollutants, the SPI model systematically accounts for multipollutant interactions, refining the accuracy of risk predictions. By incorporating cumulative risk calculations and mitigating overestimation linked to pollutant interactions, this model serves as a reliable framework for analyzing multipollutant threats in aquatic ecosystems, including five key pollutant combinations: REEs, REEs and metals, metals and pesticides, nutrients and REEs, antibiotics, and nutrients and metals in the joint ecotoxicological risk assessment of aquatic biota.[13,14,19,33,37−39] By leveraging this advanced modeling framework, this study aims to provide a comprehensive assessment of the potential ecotoxicological risks posed by Be and Tl in sedimentary environments. The detailed implementation of the SPI model, including its parametrization and application to Be and Tl risk assessment, will be elaborated in the Materials and Methods section (Section 2.5).

Given the increasing global concern over the environmental risks of emerging contaminants, this study focuses on the Pearl River Estuary, a vital ecological and economic region in southern China that is highly susceptible to metal pollution due to intense industrialization and urbanization.[33,40−43] By integrating DGT-derived bioavailability data with SPI-based probabilistic risk assessment, this study presents an innovative methodological framework for addressing the ecological threats of Be and Tl in sedimentary environments. The findings of this research will not only enhance our understanding of these underexplored contaminants but also offer critical insights for future environmental management and policy development in aquatic ecosystems worldwide.

2. MATERIALS AND METHODS

2.1. Study Area and Sample Collection. The Pearl River, flowing through southern China, ranks as China's second largest river by discharge volume. Spanning a drainage area of 446,768 km^2, it empties into the Pearl River Estuary (PRE) before reaching the South China Sea.[33,44] The PRE, a bell-shaped, semienclosed body of water along the Guangdong coast, covers an area of about 2,500 km^2.[33,45] In the western region, water depths range from 2 to 5 m, while in the eastern region, they extend to approximately 15 m.[33,44,45] The Pearl River Delta (PRD), situated in Guangdong province and surrounding the PRE, encompasses cities such as Guangzhou, Foshan, Zhaoqing, Shenzhen, Dongguan, Huizhou, Zhuhai, Zhongshan, and Jiangmen (Figure 1).

In June 2018, during the summer tide, intertidal surface sediment samples were obtained from 21 stations (Figure 1) by carefully removing them with a plastic spade. At each station, five subsamples were collected and thoroughly combined to create a representative sample. Any visible debris, such as rocks and plant fragments, was removed before the samples were freeze-dried, ground, and sieved through a 200 μm mesh for complete homogenization. The samples were then stored at −20 °C until Be and Tl analysis could be conducted.

2.2. Analytical Methods. To determine the Al_2O_3 concentration, X-ray fluorescence spectrometry (XRF) was employed. Al_2O_3 was measured because it serves as a key geochemical indicator for weathering processes and is used in Section 4.1 to help trace the natural sources of Be and Tl in sediments. A 1 g sample was compressed using an FW-5 powder compactor at a pressure of 24−28 MPa to form tablets, which were then analyzed with an XRF instrument (EDX-6000B, Skyray, China). Each batch included three standard samples (GBW07305a) and seven test samples, with each sample undergoing 10 measurements. To assess potential outliers, Grubbs' test was applied at a 95% confidence level, and no significant outliers were detected. Therefore, the average value of the 10 measurements was directly used for further analysis. The coefficients of variation remained within 10%, and the recovery for the standard samples ranged from 98 to 101%.

The bioavailable fraction of Be and Tl in sediment samples was extracted using a one-step method.[7,46] Approximately 0.1 g of sediment was placed in a 100 mL centrifuge tube, followed by the addition of 80 mL of 1 M nitric acid (HNO_3). The mixture was shaken at 250 rpm for 6 h and then centrifuged at 3000 rpm for 20 min. After centrifugation, 70 mL of the supernatant was collected and filtered through a 0.45 μm filter disk for bioavailability analysis. This one-step extraction method has been widely validated in previous studies[7,46] and is recognized for effectively assessing the labile fraction of metals in sediments. It provides a reliable measure of metal availability under environmentally relevant conditions. The bioavailable fraction of Be and Tl represents the portion that is readily mobilized under natural conditions and thus poses potential ecological risks. Unlike total concentrations, bioavailable concentrations provide insight into metal mobility and bioaccumulation potential in aquatic environments. High bioavailability suggests increased environmental risks, making this parameter crucial for assessing the metal impact on aquatic ecosystems.

The concentrations of total Be and Tl in sediment samples were determined following the procedures outlined in the China National Standard "Soil quality—Determination of 22 elements—Dissolution with acids and inductively coupled plasma mass spectrometry" (Standard No. 20205108-T-326), which is currently under approval and expected to be officially published soon. Approximately 0.1 g of the sample (accurate to 0.1 mg) was weighed and placed in a polytetrafluoroethylene digestion tube. The sample was moistened with a small amount of water, followed by the addition of 3 mL of nitric acid (1.42 g/mL), 3 mL of hydrofluoric acid (1.15 g/mL), and 1 mL of perchloric acid (1.68 g/mL). The tube was heated on a graphite digestion apparatus at 120 °C for 0.5 h (excluding the heating time). The temperature was then increased to 140 °C and held for 1 h, followed by a further increase to 160 °C for 2 h, until the sample emitted white fumes. After slight cooling, 2 mL of hydrofluoric acid, 0.5 mL of perchloric acid, and 3 mL of nitric acid were added, and the mixture was heated at 160 °C for 2 h. Once the acids had completely evaporated, 2 mL of 2 mol/L hydrochloric acid was added to dissolve the residue. The solution was then diluted to 50 mL with ultrapure water, thoroughly mixed, and immediately transferred to a clean, dry polyethylene centrifuge tube for storage until analysis.

The concentration of Be was measured using inductively coupled plasma mass spectrometry (ICP-MS, Agilent 700 series). Blanks and the Chinese National Standard reference material (GBW07314) were analyzed at regular intervals (one blank and one standard per four samples) to ensure precision and accuracy. The recovery rates for samples spiked with standards ranged from 97 to 102%. The lower limits of quantification (LOQs) for Be and Tl in sediment samples were 0.02 and 0.01 mg/kg, respectively, based on method validation using the Chinese National Standard reference material (GBW07314).

https://doi.org/10.1021/acsestwater.5c00307
ACS EST Water 2025, 5, 5145−5156

2.3. Transformation of Exposure Data Units. The units of toxicity data and exposure data are mg/L and mg/kg, respectively. To determine probabilistic ecological risk, the unit of exposure data needs to be converted. It is assumed that the density of sediment water content (SWC) is 1 g/cm^3 and that the concentration of bioavailable Be or Tl in sediments can be fully transferred into the SWC. The concentration of bioavailable Be in dry sediments can be converted using the following eq 1:[7]

$$C_w = \frac{C_s}{W_c} \times 1000 \quad (1)$$

where C_w is concentration of bioavailable Be or Tl in water (mg/L), C_s is concentration of bioavailable Be or Tl in dry sediments (mg/kg), and W_c is SWC (%).

2.4. Assessment of Pollution Indices. The geoaccumulation index (I_{geo}) established by Müller[47] was employed in this study. The I_{geo} is calculated using the following eq 2:

$$I_{geo} = \log_2\left(\frac{C_n}{1.5B_n}\right) \quad (2)$$

where C_n represents the concentration of Be or Tl in the sediment sample and B_n is the background concentration of Be or Tl. The constant 1.5 compensates for lithogenic variations in the site's background concentrations. Since background values of Be and Tl in the study area are unavailable and considering that the Pearl River Estuary receives substantial sediment input from the Pearl River Basin, we adopted the values from Guangdong province soils, specifically 1.61 mg/kg for Be and 0.682 mg/kg for Tl, as reported by CEMS.[48] This approach is reasonable because the sediments in the estuary primarily originate from upstream soil erosion and transport, making the geochemical characteristics of the basin's soil a suitable reference.[49−51] A similar approach has been adopted in previous estuarine studies where sediment background values were unavailable.[7,36] According to the classification by Gu et al.,[15] the I_{geo} is categorized into seven levels: $I_{geo} \leq 0$ for unpolluted, $0 < I_{geo} \leq 1$ for slightly polluted, $1 < I_{geo} \leq 2$ for moderately polluted, $2 < I_{geo} \leq 3$ for moderate to severe pollution, $3 < I_{geo} \leq 4$ for severely polluted, $4 < I_{geo} \leq 5$ for extremely severe pollution, and $I_{geo} > 5$ for extreme pollution.

The pollution load index (PLI) as developed by Tomlinson et al.[52] was utilized. The PLI is calculated by taking the nth root of the product of the concentration factors (CF) for each metal:

$$PLI = (CF_1 \times CF_2 \ldots CF_n)^{1/n} \quad (3)$$

The CF is determined as the ratio between the concentration of each metal and its corresponding background value. Based on Gu et al.,[15] the PLI is categorized into several levels: unpolluted ($0 < PLI \leq 1$), slightly polluted ($1 < PLI \leq 2$), moderately polluted ($2 < PLI \leq 3$), moderate to high pollution ($3 < PLI \leq 4$), highly polluted ($4 < PLI \leq 5$), and extremely high pollution ($PLI > 5$).

2.5. SPI Model Framework for Combined Ecotoxicological Risk Assessment. The SPI model utilizes a systematic and probabilistic methodology to evaluate the combined ecological risks of multiple pollutants, including inorganic and organic contaminants, in aquatic ecosystems.[13,14,19,33,37,38] By incorporating SSD, PRA, and IEP, this approach ensures a thorough assessment of cumulative risks while minimizing the potential for overestimation caused by pollutant interactions (Figure 2). The model is structured into three fundamental steps (Figure 2).

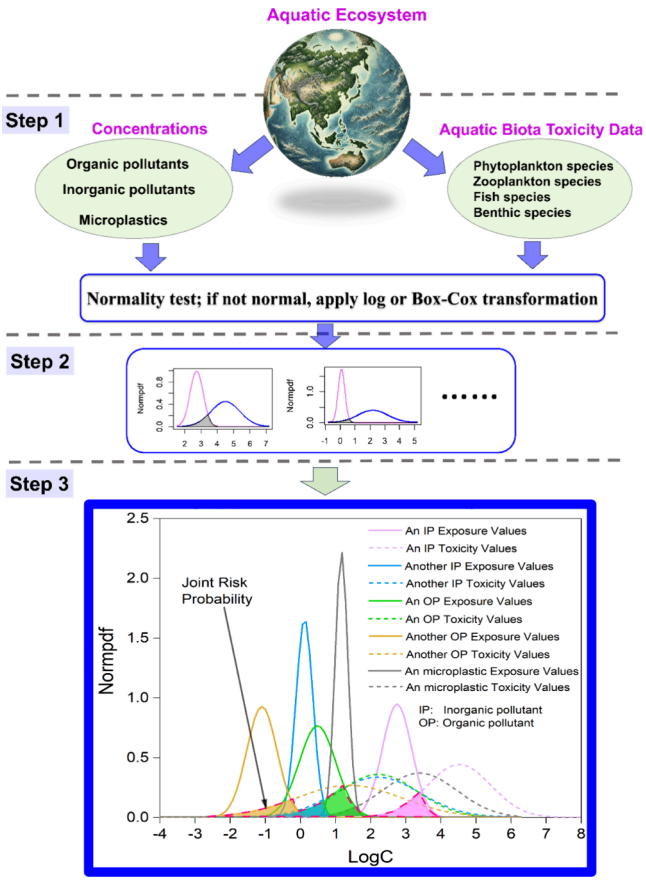

Figure 2. Schematic representation of the SPI model framework for quantitative probabilistic ecotoxicological risk assessment. This model integrates species sensitivity distribution (SSD), probabilistic risk assessment (PRA), and the inclusion-exclusion principle (IEP) to evaluate cumulative ecological risks posed by multiple pollutants. The main steps include (1) data collection and compilation of toxicity information, (2) calculation of risk probability through PRA, and (3) joint risk assessment using IEP to account for pollutant interactions and minimize overestimation.

2.5.1. Step 1: Pollutant Concentration and Toxicity Data Collection. Environmental exposure concentrations of Be and Tl were obtained from sediment samples by converting weak acid-exchangeable sediment concentrations (mg/kg) into aqueous-phase concentrations (mg/L), which provided a practical alternative for assessing their bioavailability (Section 2.3). Acute toxicity data for Be and Tl were sourced from the USEPA ECOTOX database, covering algae, crustaceans, mollusks, and fish species (https://cfpub.epa.gov/ecotox/). These data are summarized in Table S1, with detailed toxicity values and aquatic species listed in Tables S2 and S3. To ensure normality, toxicity data were tested and log-transformed, or Box−Cox transformed if necessary, to enhance the robustness of the risk assessment model.

2.5.2. Step 2: Ecotoxicological Risk Assessment Using SSD and PRA. To quantify the probability of ecological risks associated with individual pollutants, a PRA approach was employed.[13,14,33,53] Probability density functions (PDFs) were constructed based on pollutant concentration data and SSD derived from toxicity data for Be and Tl. These PDFs depict

https://doi.org/10.1021/acsestwater.5c00307
ACS EST Water 2025, 5, 5145−5156

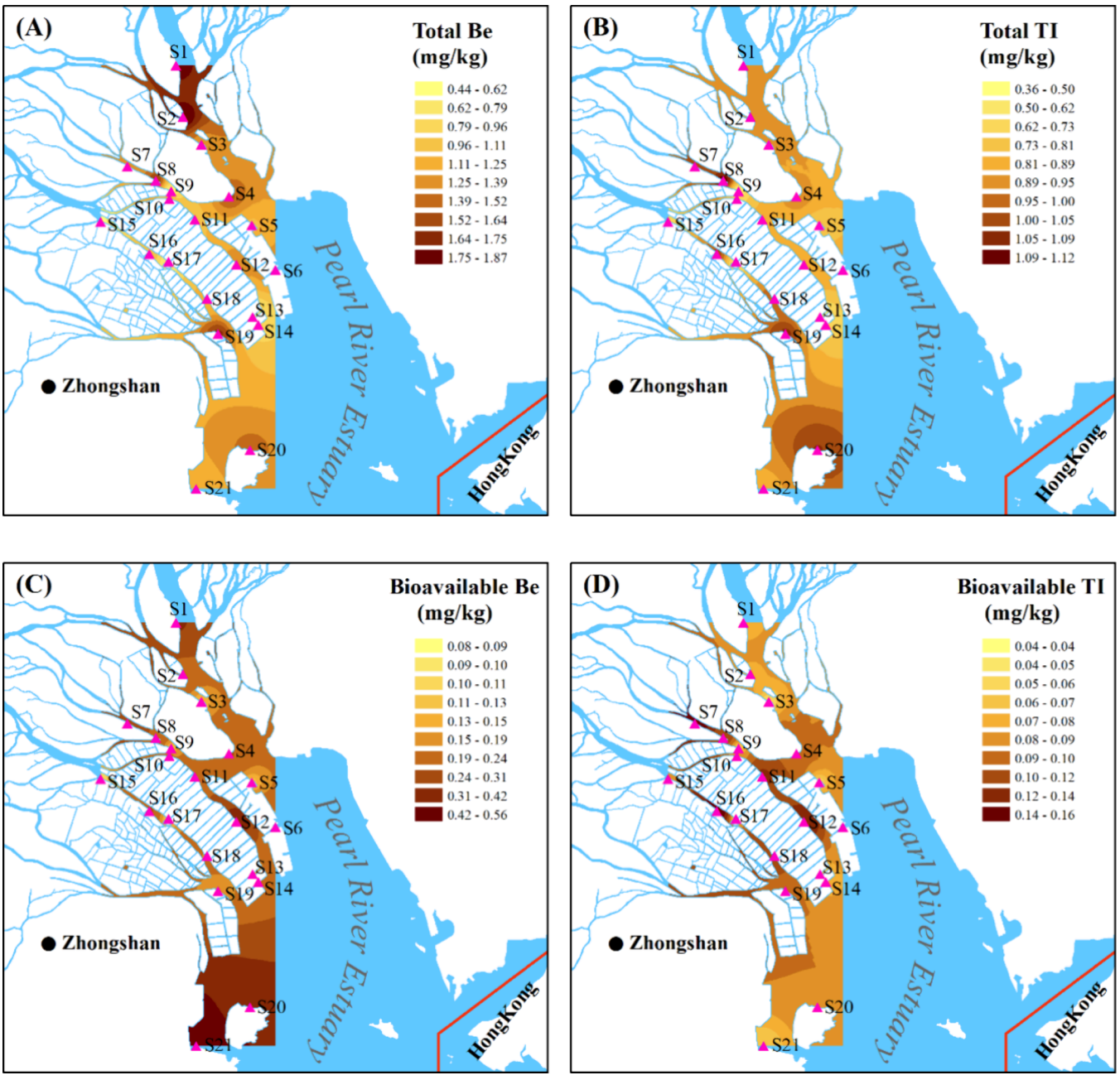

Figure 3. Spatial distributions of (A) total Be, (B) total TI, (C) bioavailable Be, and (D) bioavailable TI in the Pearl River Estuary intertidal zone.

the likelihood of adverse effects on aquatic organisms under different exposure levels. If the toxicity or environmental concentration data deviate from normality, then log-transformation or Box−Cox transformation is applied to correct skewness.

The ecotoxicological risk probability for each pollutant was determined by analyzing the intersection between the probability density curves of exposure concentrations and SSD. The probability of adverse effects, represented as the potentially affected fraction (PAF), was obtained through statistical integration using R software. This approach quantifies the likelihood that a pollutant's concentration exceeds species toxicity thresholds, thereby indicating its ecological risk.

2.5.3. Step 3: Combined Risk Assessment Using the IEP. To assess the combined ecotoxicological risks of Be and Tl, the SPI model incorporates the IEP, a probability-driven method that considers overlapping toxic effects while avoiding overestimation. The overall ecotoxicological risk probability is calculated using the IEP, as expressed in eq 4:[13,14,33,53]

$$\begin{aligned}&\Phi[A_1 + A_2 + \ldots + A_n]\\ &= \sum_{i-1}^{n} \Phi[A_i] - \sum_{i1<i2} \Phi[A_{i1}A_{i2}] + \ldots\\ &\quad + (-1)^{r+1} \sum_{i1<i2<\ldots<ir} \Phi[A_{i1}A_{i2}\ldots A_{ir}] + \ldots\\ &\quad + (-1)^{n+1}\Phi[A_1 + A_2 + \ldots + A_n] \end{aligned} \quad (4)$$

where Φ represents the probability function; $\Phi[A_1 + A_2 + \ldots + A_n]$ denotes the joint ecological risk probability of pollutants A_1, A_2, ..., A_n, indicating the likelihood that at least one pollutant will pose a risk; the term $\sum_{i-1}^{n} \Phi[A_i]$ sums the

https://doi.org/10.1021/acsestwater.5c00307
ACS EST Water 2025, 5, 5145−5156

individual probabilities of each pollutant; the expression $-\sum_{i1<i2}\Phi[A_{i1}A_{i2}]$ subtracts the probability of pairwise intersections to correct for overestimation; the alternating sum and subtraction term $(-1)^{r+1}\sum_{i1<i2<\ldots<ir}\Phi[A_{i1}A_{i2}\ldots A_{ir}]$accounts for overlapping effects among multiple pollutants; finally, $(-1)^{n+1}\Phi[A_1 + A_2 + \ldots + A_n]$ ensures proper adjustment for the total intersection of all n pollutants, yielding an accurate cumulative risk probability.

2.6. Statistical Analysis. The nonmetric multidimensional scaling (NMDS) analysis was conducted using the vegan package in R-4.3.2 for Windows (64 bit), while the overlap areas between exposure and toxicity data were calculated directly in R-4.3.2 for Windows (64 bit). The Kolmogorov−Smirnov (K−S) test was conducted using SPSS 19.0 for Windows.

3. RESULTS

3.1. Distributions of Total Be and Tl. The spatial distribution maps of total Be and total Tl in surface sediments of the Pearl River Estuary intertidal zone are shown in Figure 3A,B and Table S4. The total concentrations of Be ranged from 0.44 to 1.87 mg/kg, with an average value of 1.22 mg/kg. The spatial distribution of total Be exhibited significant regional variation. Elevated concentrations were observed primarily in the northern and western sites, such as S1, S2, S8, and S19, where total Be levels notably exceeded the average, ranging from 1.81 to 1.87 mg/kg. In contrast, lower concentrations were found in the southeastern sites, including S9, S13, and S14, with total Be concentrations ranging from 0.44 to 0.95 mg/kg, suggesting a lower degree of enrichment in these areas.

Similarly, the total concentrations of Tl ranged from 0.36 to 1.12 mg/kg, with an average of 0.86 mg/kg. The spatial distribution of Tl showed both similarities to and differences from that of Be. High total Tl concentrations were concentrated in the central and western sites, such as S7, S8, S19, and S20, with values ranging from 1.04 to 1.12 mg/kg, all exceeding the average. Conversely, the southeastern sites, particularly S9 and S13, exhibited the lowest total Tl concentrations, at 0.36 and 0.46 mg/kg, respectively, indicating relatively lower Tl levels in these areas.

In general, the analysis of spatial distribution for both total Be and Tl highlighted that certain sites, such as S8 and S19, showed higher concentrations of these elements. This observation suggested the potential influence of specific pollution sources or natural enrichment processes in these areas. These distribution patterns provided important insights for further environmental monitoring and pollution source investigation.

3.2. Distributions of Bioavailable Be and Tl. The distributions of bioavailable Be and Tl in the surface sediments of the Pearl River Estuary intertidal zone are illustrated in Figure 3C,D and Table S4. The distributions exhibited significant spatial variability. Bioavailable Be concentrations ranged from 0.08 to 0.56 mg/kg, with an average of 0.23 mg/kg, while bioavailable Tl concentrations varied from 0.04 to 0.16 mg/kg, with an average of 0.09 mg/kg. Elevated levels of Be were concentrated in the southern part of the estuary, particularly around station S21, where the highest concentration of 0.56 mg/kg was observed. In contrast, Be concentrations were lower in the central and northern regions, with the lowest value of 0.08 mg/kg recorded at station S9. For Tl, higher concentrations were found in the central part of the estuary, especially near stations S7 and S16, where concentrations reached 0.16 mg/kg at both locations. The southern region showed lower Tl levels, with the minimum concentration of 0.04 mg/kg observed at station S9.

The spatial distributions of these metals were influenced by several factors. Although the total concentrations of Be and Tl in the sediments primarily originated from natural weathering processes, tidal currents and hydrodynamic conditions play a crucial role in their deposition and migration, leading to variations in metal concentrations across different regions (Section 4.1). Additionally, the presence of nearby industrial activities and discharge outlets may contribute to localized increases in metal concentrations. For instance, the southern and central regions might experience higher levels of human activity, which could enhance the accumulation of Be and Tl. Furthermore, the sediment type and grain size distribution affect heavy metal adsorption and accumulation. Finer sediments typically exhibit higher adsorption capacity for heavy metals, which may explain the increased concentrations observed in certain areas.

When comparing the distribution of bioavailable Be and Tl with their total concentrations, both similarities and differences emerged. High-value areas for bioavailable Be and Tl often overlapped with regions of high total metal concentrations. For example, in the western and northern areas, such as stations S1, S2, S8, and S19, high total metal concentrations coincided with relatively high bioavailability, suggesting that sediment characteristics or local environmental conditions in these regions might have enhanced metal availability to organisms. However, the distribution of bioavailable Be and Tl also showed trends that differed from those of total metal concentrations. For instance, at station S20, despite high total concentrations of Be and Tl, their bioavailability was relatively low. Conversely, at station S21, although total concentrations were not high, bioavailability reached its peak. These discrepancies might have been related to the physicochemical properties of sediments, such as finer particle size and higher organic matter content, which could have enhanced metal adsorption and bioavailability. Additionally, changes in redox conditions might have facilitated the release and utilization of metals in specific areas.

4. DISCUSSION

4.1. Source of Be and Tl. Researches have demonstrated that nonmetric multidimensional scaling (NMDS) combined with geographic information system (GIS) techniques is an effective method for identifying pollutant sources.[54−56] To determine the sources of total Be and total Tl, we employed NMDS and GIS to generate continuous spatial distribution maps based on NMDS scores. The NMDS results, illustrated in Figure 4A, indicate that the metals under study originate from two distinct sources. Specifically, NMDS1 accounts for 54.64% of the data variance, while NMDS2 explains 2.27%. Based on these findings, we calculated NMDS1 scores for each site to create spatial distribution maps (Figure 4B). While NMDS1 primarily distinguishes metals based on their geochemical affinities, NMDS2 captures an additional gradient related to variations in metal behavior. Additionally, NMDS2 was found to be associated with Cu, Pb, and Zn. Our prior research on samples from the same sites indicated that Cu, Pb, and Zn in this area primarily derive from human activities.[57]

https://doi.org/10.1021/acsestwater.5c00307
ACS EST Water 2025, 5, 5145−5156

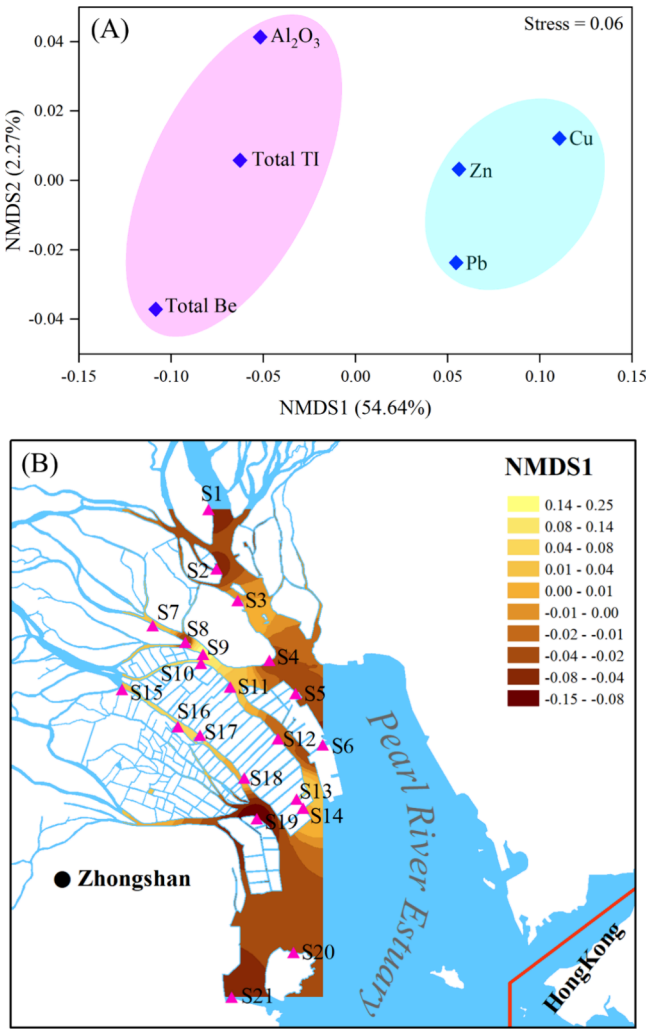

Figure 4. Nonmetric multidimensional scaling (NMS) ordination of metals using the Bray−Curtis similarity matrix (A) and spatial distribution of scores of NMS1 (B) in surface sediments of the Pearl River Estuary intertidal zone.

Therefore, NMDS2 likely reflects anthropogenic influences, particularly related to industrial discharges and urban runoff.

NMDS1 reveals a strong affinity between Be, Tl, and Al_2O_3. In geochemical contexts, Be and Tl typically exhibit a strong affinity with Al, particularly in minerals formed through weathering.[1,58−63] Be is primarily found in nature as beryllium aluminum silicate, while Tl commonly occurs with aluminum silicates or other aluminum oxides.[1,64−67] As rocks undergo weathering, minerals containing these elements gradually break down, releasing Be and Tl, which then combine with Al_2O_3 in sedimentary environments. This suggests that NMDS1 is primarily governed by lithogenic processes, where Be and Tl are mobilized from parent rocks through natural weathering. Consequently, the strong correlation between Be, Ti, and Al_2O_3 in sediments suggests that these elements predominantly originate from natural weathering processes. Unlike NMDS2, which highlights anthropogenic influences, NMDS1 reflects the geochemical background of the study area. This affinity indicates that weathering plays a crucial role in the distribution and cycling of these elements, as opposed to industrial emissions or other human activities. Therefore, we conclude that Be and Ti are primarily sourced from natural weathering. Sites with higher NMDS1 scores are generally associated with natural weathering processes. The spatial distribution of NMDS1 scores suggests that Be and Tl at sites S3, S7, S9, S10, S11, S13, S15, S16, S17, and S18 are more strongly influenced by natural weathering (Figure 4B). Meanwhile, sites with relatively higher NMDS2 scores may indicate localized anthropogenic inputs, highlighting the need for further investigation into potential industrial or urban sources.

4.2. Pollution Degree Assessment. The I_{geo} values for Be and Tl in this study are illustrated in Figure 5A and Figure 5B, respectively. The I_{geo} index for Be revealed that this element was uniformly categorized as "unpolluted" across all sites, with values showing slight spatial variations. The highest I_{geo} value was found at site S2 in the northern part of the region (−0.37), while the lowest was observed at site S9 in the central area (−2.46) (Figure 5A,D). This pattern suggested that Be concentrations were generally low and evenly distributed, with no significant localized accumulation detected.

In contrast, the I_{geo} index for Tl indicated slight spatial variability, with some sites showing values slightly above 0, signaling mild pollution. Notably, site S8 displayed the highest I_{geo} value (0.13), pointing to a relatively higher concentration of Tl in this area (Figure 5B,D). Other sites with elevated Tl levels included S7, S16, S18, S19, and S20, primarily located in the central-southern and southeastern parts of the study area (Figure 5B,D). This distribution suggested that Tl pollution, while generally mild, was more pronounced in these regions.

To evaluate the combined pollution of Be and Tl in the study area, the PLI was used. The PLI values derived from this study are shown in Figure 5C. Site S8 stood out with the highest PLI value of 1.30, indicating mild combined pollution, which aligned with the higher Tl concentrations observed (Figure 5C,D). In contrast, sites such as S9, S13, S14, and S15 exhibited lower PLI values, suggesting that these areas were either unpolluted or only slightly polluted (Figure 5C,D).

Overall, the distribution of Be was fairly uniform and low across the study area, while Tl showed slight enrichment at specific sites, particularly in the central-southern and southeastern regions. The PLI distribution further underscored these findings, highlighting areas where environmental monitoring and management efforts should have been prioritized to mitigate potential pollution risks.

4.3. Combined Ecotoxicological Risk Assessment Using an SPI Model. To evaluate the combined effects of Be and Tl, potential bioavailable concentrations were determined using toxicity data, and the species sensitivity distribution (SSD) method was applied to predict probabilistic biological risks. It is important to note that the Be and Tl concentrations used in this study represent potential bioavailable concentrations rather than true bioavailable concentrations. These estimations are based on weak acid-exchangeable fractions, which approximate bioavailability but may not fully capture the fraction readily available for biological uptake. As a result, the ecological risk probabilities estimated in this study may be overestimated. The distribution of exposure concentrations and toxicological effects on sensitive species was analyzed using the K−S test. The results indicated that the transformed exposure and toxicity data followed a normal distribution ($p > 0.05$) (Table S5). Table S5 also presents the mean values, standard deviations (SDs), and K−S test results for Be and Tl. These values were then used to construct a normal probability distribution curve for risk analysis (Figure 6A,B).

https://doi.org/10.1021/acsestwater.5c00307
ACS EST Water 2025, 5, 5145−5156

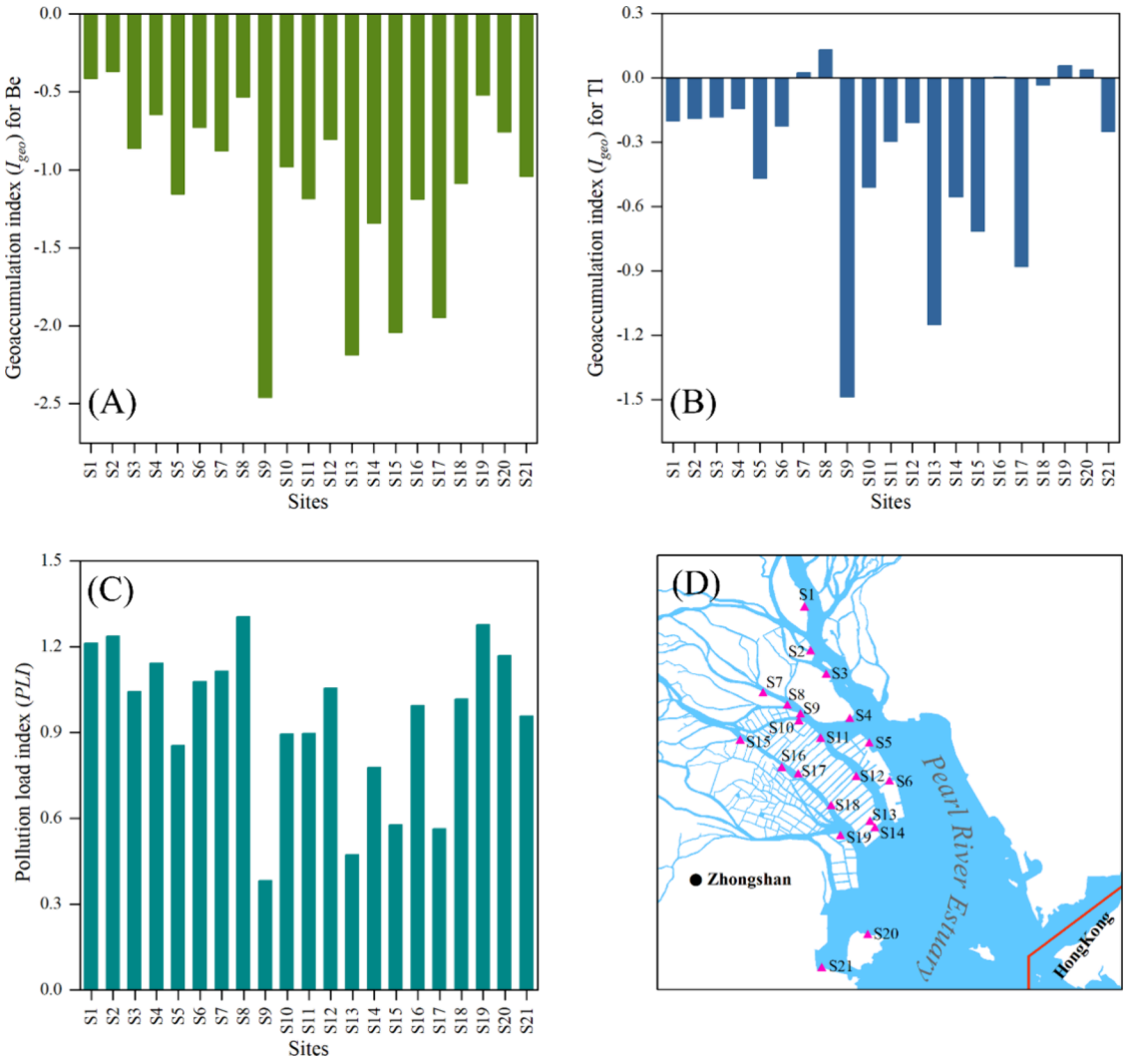

Figure 5. Geoaccumulation index (I_{geo}) for Be and Tl (A, B), pollution load index (PLI) (C) in surface sediments of the Pearl River Estuary intertidal zone, and sampling sites within the estuary (D).

The study calculated the overlap between the exposure distributions and the corresponding toxicity data for Be and Tl (Figure 6A,B). The ecological risk probabilities were found to be 33.77% for Be and 24.92% for Tl. However, due to the lack of standardized sediment toxicity data for Be and Tl, this study relied on water-based toxicity values for risk estimation. While this approach is commonly used in probabilistic risk assessments, it introduces uncertainties due to differences in exposure pathways and bioavailability between sediment and water systems. If direct sediment toxicity data become available in the future, then they should be incorporated to improve the accuracy of ecological risk assessments. By summing these probabilities, as described in previous studies,[13,33] toxic effect probabilities were used to estimate the cumulative biological risks associated with Be and Tl mixtures. This analysis revealed a 37.05% probability of combined toxic effects on aquatic organisms in the surface sediments of the Pearl River Estuary intertidal zone (Figure 6C). According to the ecotoxicological risk classification guidelines recommended by the U.S. EPA,[68,69] combined ecotoxicological risks are categorized into four levels: 8, 21, 49, and 73%. However, given that joint risk probabilities in major natural water bodies in China generally exceed 10%, we propose ecological risk alert thresholds at 25 and 50%. A probability exceeding 25% warrants a mild risk alert, prompting investigations into the causes, while a probability over 50% necessitates a high-risk alert, leading to immediate investigation and intervention. The risk level observed in this study, ranging from 21 to 49%, surpasses the mild risk alert threshold of 25%, indicating a moderate ecotoxicological risk and warranting further investigation into potential sources and impacts. However, it is acknowledged that ecological risk estimation involves inherent uncertainties, particularly when extrapolating from water-based toxicity data to sediment environments. To improve future risk assessments, integrating site-specific bioassays, equilibrium-based bioavailability models, and sediment toxicity thresholds is recommended.

5. ENVIRONMENTAL SIGNIFICANCE

This study reveals the overlooked ecotoxicological risks of naturally occurring Be and Tl in sediments, demonstrating a 37.05% probability of ecological hazard in the Pearl River Estuary. These findings challenge the conventional assumption that metal contamination is solely anthropogenic, emphasizing the need for improved risk assessments of naturally sourced pollutants. By integrating a novel bioavailability conversion

https://doi.org/10.1021/acsestwater.5c00307
ACS EST Water 2025, 5, 5145−5156

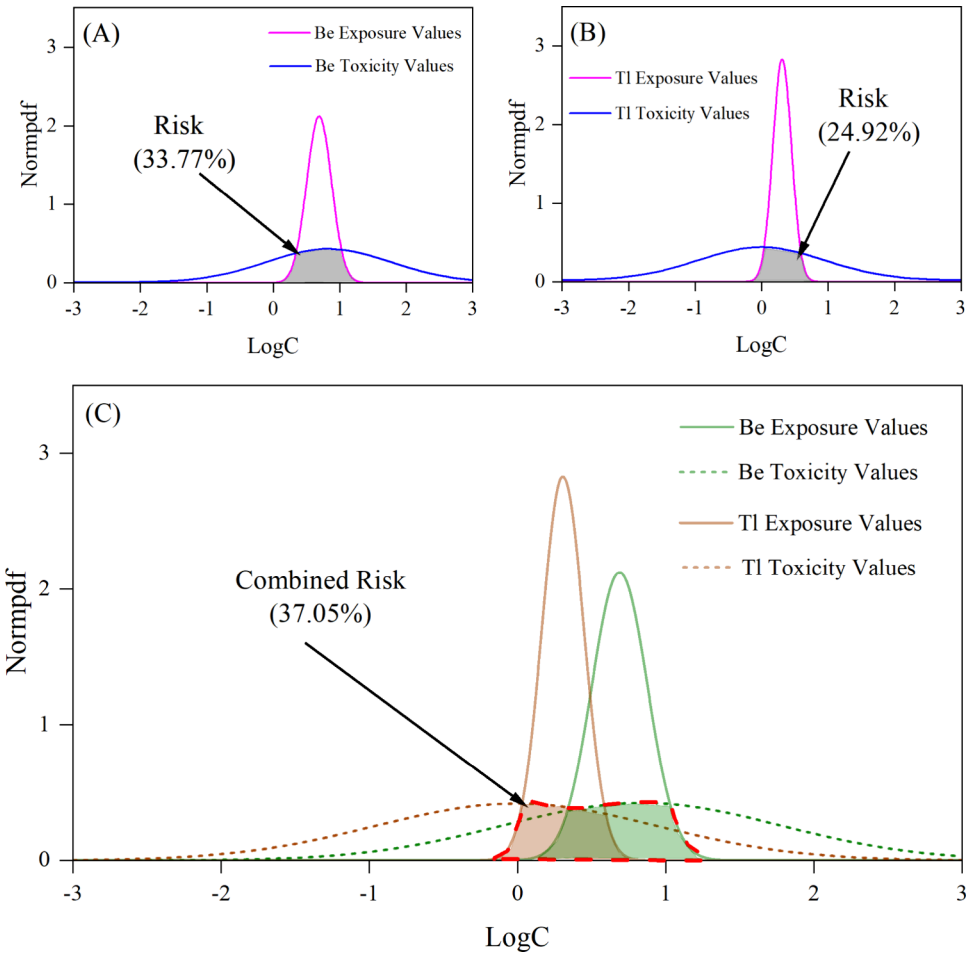

Figure 6. Density distributions of exposure and toxicity probabilities for Be and Tl (A, B) and the combined probabilistic ecotoxicological risk of Be and Tl to aquatic biota (C) in surface sediments of the Pearl River Estuary intertidal zone were analyzed using logarithmic transformation (LogC, base 10). In panel C, the red polygon represents the combined toxicity.

method with the SPI model, this research provides a practical alternative to DGT for Be and Tl assessment. The results offer critical insights for environmental monitoring, risk management, and policy development, ensuring better protection of estuarine and coastal ecosystems from emerging contaminant threats.

■ ASSOCIATED CONTENT

Supporting Information

The Supporting Information is available free of charge at https://pubs.acs.org/doi/10.1021/acsestwater.5c00307.

Acute toxicity data for studied metals (Tables S1−S3), including species-specific data for beryllium and thallium for algae, crustaceans, mollusks, and fish; concentrations of total and bioavailable metals (Be, Tl, Cu, Pb, Zn, and Al_2O_3) in surface sediments of the Pearl River Estuary (Table S4); and exposure and toxicity data with log-transformed distribution parameters, standard deviations, and Kolmogorov−Smirnov test results (Table S5) (PDF)

■ AUTHOR INFORMATION

Corresponding Author

Yang-Guang Gu − *South China Sea Fisheries Research Institute, Chinese Academy of Fishery Sciences, Guangzhou 510300, China; Key Laboratory of Fishery Ecology and Environment, Guangdong Province, Guangzhou 510300, China;* orcid.org/0000-0003-2314-0463; Phone: +86-20-89102080; Email: hydrobio@163.com; Fax: +86-20-84451442

Authors

Yan-Peng Gao − *Institute of Environmental Health and Pollution Control, Guangdong University of Technology, Guangzhou 510006, China*

Rui-Ze Liang − *College of Oceanography, Hohai University, Nanjing 245700, China*

Richard W. Jordan − *Faculty of Science, Yamagata University, Yamagata 990-8560, Japan*

Shi-Jun Jiang − *State Key Laboratory of Marine Resource Utilization in South China Sea, Hainan University, Haikou 570228, China*

Complete contact information is available at: https://pubs.acs.org/10.1021/acsestwater.5c00307

Notes

The authors declare no competing financial interest.

■ ACKNOWLEDGMENTS

This study was supported by the National Natural Science Foundation of China (42322704), Guangdong Basic and

Applied Basic Research Foundation (2023B1515020078), National Key R&D Program of China (2019YFD0901105), and Central Public-Interest Scientific Institution Basal Research Fund, CAFS (2023TD15).

REFERENCES

(1) Bolan, S.; Wijesekara, H.; Tanveer, M.; Boschi, V.; Padhye, L. P.; Wijesooriya, M.; Wang, L.; Jasemizad, T.; Wang, C.; Zhang, T.; Rinklebe, J.; Wang, H.; Lam, S. S.; Siddique, K. H. M.; Kirkham, M. B.; Bolan, N. Beryllium contamination and its risk management in terrestrial and aquatic environmental settings. *Environ. Pollut.* **2023**, *320*, No. 121077.

(2) Gu, Y. G. Calculation of beryllium toxic factor for potential ecological risk evaluation: A case study. *Environmental Technology & Innovation* **2021**, *21*, No. 101361.

(3) Liu, J.; Yan, G. Z.; Huo, Z. H.; Mo, Y. C.; Wen, Y. T.; Liu, W. Z.; Zhou, H. Y.; Yan, B.; Lin, Z. Thallium's threat to aquatic life: Stage-specific toxicity in zebrafish embryos and larvae. *Environment & Health* **2024**, *2* (3), 114−125.

(4) Markich, S. J.; Hall, J. P.; Dorsman, J. M.; Brown, P. L. Thallium toxicity to temperate and tropical marine organisms: Derivation of water quality guidelines to protect marine life. *Mar. Pollut. Bull.* **2023**, *192*, No. 114964.

(5) Wei, X. R.; Li, X.; Liu, P.; Li, L.; Chen, H. X.; Li, D.; Liu, J.; Xie, L. T. Integrated physiological, biochemical, and transcriptomic analysis of thallium toxicity in zebrafish (Danio rerio) larvae. *Science of The Total Environment* **2023**, *859*, No. 160265.

(6) Zhong, Q. H.; Qi, J. Y.; Liu, J.; Wang, J.; Lin, K.; Ouyang, Q. E.; Zhang, X.; Wei, X. D.; Xiao, T. F.; El-Naggar, A.; Rinklebe, J. Thallium isotopic compositions as tracers in environmental studies: A review. *Environ. Int.* **2022**, *162*, No. 107148.

(7) Gu, Y. G.; Wang, L. G.; Gao, Y. P. Beryllium in riverine/estuarine sediments from a typical aquaculture wetland, China: Bioavailability and probabilistic ecological risk. *Mar. Pollut. Bull.* **2018**, *137*, 549−554.

(8) Stepanyan, A.; Arakelyan, A.; Schug, J. Transcriptome alterations in long-term mining region residents: Insights into immune response and molecular pathways. *Environ. Int.* **2025**, *197*, No. 109344.

(9) Sánchez-Chapul, L.; Santamaría, A.; Aschner, M.; Ke, T.; Tinkov, A. A.; Túnez, I.; Osorio-Rico, L.; Galván-Arzate, S.; Rangel-López, E. Thallium-induced DNA damage, genetic, and epigenetic alterations. *Front. Genet.* **2023**, *14*, No. 1168713.

(10) Ponce-Hernández, A.; Carranza-Álvarez, C.; Ceballos-Maldonado, J. G.; Rubio-Gómez, J. A.; Martínez-Soto, D. Overview of the heavy metal contamination in Mexico: sources of the contamination and issues in human health. *Environmental Geochemistry and Health* **2025**, *47* (3), 82.

(11) Das, S.; VishnuRadhan, R. *Effect of trace metals on aquatic invertebrates: Dynamics and repercussions*. In Springer, Berlin Heidelberg: Berlin, Heidelberg, 2024; pp 1−40.

(12) Zitoun, R.; Marcinek, S.; Hatje, V.; Sander, S. G.; Völker, C.; Sarin, M.; Omanović, D. Climate change driven effects on transport, fate and biogeochemistry of trace element contaminants in coastal marine ecosystems. *Communications Earth & Environment* **2024**, *5* (1), 560.

(13) Gu, Y. G.; Gao, Y. P.; Chen, F.; Huang, H. H.; Yu, S. H.; Jordan, R. W.; Jiang, S. J. Risk assessment of heavy metal and pesticide mixtures in aquatic biota using the DGT technique in sediments. *Water Res.* **2022**, *224*, No. 119108.

(14) Gu, Y.-G.; Ma, C.; Jordan, R. W.; Jiang, S.-J.; Wang, M. Nutrients and rare earth elements in surface sediments of Hongze Lake (China) using the DGT technique: spatial distribution pattern and probabilistic risk. *ACS ES&T Water* **2024**, *4* (5), 2247−2258.

(15) Gu, Y. G.; Wang, X. N.; Wang, Z. H.; Jordan, R. W.; Jiang, S. J. Rare earth elements in sediments from a representative Chinese mariculture bay: Characterization, DGT-based bioaccessibility, and probabilistic ecological risk. *Environ. Pollut.* **2023**, *335*, No. 122338.

(16) Liu, J.; Ouyang, Q. E.; Wang, L. L.; Wang, J.; Zhang, Q.; Wei, X. D.; Lin, Y. Y.; Zhou, Y. T.; Yuan, W. H.; Xiao, T. F. Quantification of smelter-derived contributions to thallium contamination in river sediments: Novel insights from thallium isotope evidence. *Journal of Hazardous Materials* **2022**, *424*, No. 127594.

(17) Li, S. L.; Goldstein, S. L.; Raymo, M. E. Neogene continental denudation and the beryllium conundrum. *Proc. Natl. Acad. Sci. U. S. A.* **2021**, *118* (42), No. e2026456118.

(18) Kastury, F.; Besedin, J.; Betts, A. R.; Asamoah, R.; Herde, C.; Netherway, P.; Tully, J.; Scheckel, K. G.; Juhasz, A. L. Arsenic, cadmium, lead, antimony bioaccessibility and relative bioavailability in legacy gold mining waste. *Journal of Hazardous Materials* **2024**, *469*, No. 133948.

(19) Gu, Y. G.; Huang, H. H.; Jiang, S. J.; Gong, X. Y.; Liao, X. L.; Dai, M. Appraising ecotoxicological risk of mercury species and their mixtures in sediments to aquatic biota using diffusive gradients in thin films (DGT). *Science of The Total Environment* **2022**, *825*, No. 154069.

(20) Gu, Y. G.; Wang, Q.; Li, Y. F. An emerging contaminant in sediments of the largest wetland ecosystem in northern China: Bioaccessibility and probabilistic adverse effects on aquatic biota. *Journal of Geochemical Exploration* **2020**, *219*, No. 106652.

(21) Oliveira, L. A.; Santos, J. L. O.; Teixeira, L. S. G. Determination of thallium in water samples via solid sampling HR-CS GF AAS after preconcentration on chromatographic paper. *Talanta* **2024**, *266*, No. 124945.

(22) Zhao, X.; Lei, Z. W.; Hou, H. S.; Lin, G. Q.; Sun, Y. G.; Li, H. S.; Yang, X. P.; Su, Y. C.; Ali, K. M. Y.; Hu, E.; Wang, H. Q.; Wang, Q. L.; Hu, F. Purification of high−toxicity beryllium−containing water resources using carbon dot−enhanced phosphoric acid/chitosan composite gels. *Sep. Purif. Technol.* **2025**, *358*, No. 130299.

(23) Zhang, Y. Q.; Zhang, M.; Yu, W. X.; Li, J. Y.; Kong, Y. Ecotoxicological risk ranking of 19 metals in the lower Yangtze River of China based on their threats to aquatic wildlife. *Science of The Total Environment* **2022**, *812*, No. 152370.

(24) Cupe-Flores, B.; Mendes, M.; Panigrahi, B.; Liber, K. Delineating effluent exposure and cumulative ecotoxicological risk of metals downstream of a Saskatchewan Uranium mill using autonomous sensors. *Environ. Toxicol. Chem.* **2022**, *41* (7), 1765−1777.

(25) US EPA *Toxicological review of beryllium and compounds*. In USEPA: 1998; p 94. https://iris.epa.gov/static/pdfs/0012tr.pdf. (accessed 2025−07−30).

(26) Rickwood, C. J.; King, M.; Huntsman-Mapila, P. Assessing the fate and toxicity of Thallium I and Thallium III to three aquatic organisms. *Ecotoxicology and Environmental Safety* **2015**, *115*, 300−308.

(27) Gordon, T.; Bowser, D. Beryllium: genotoxicity and carcinogenicity. *Mutation Research/Fundamental and Molecular Mechanisms of Mutagenesis* **2003**, *533* (1), 99−105.

(28) Zhang, H.; Davison, W. Use of diffusive gradients in thin-films for studies of chemical speciation and bioavailability. *Environmental Chemistry* **2015**, *12* (2), 85−101.

(29) Li, C.; Ding, S. M.; Chen, M. S.; Zhong, Z. L.; Sun, Q.; Wang, Y. Visualizing biogeochemical heterogeneity in soils and sediments: A review of advanced micro-scale sampling and imaging methods. *Critical Reviews in Environmental Science and Technology* **2023**, *53* (12), 1229−1253.

(30) Amato, E. D.; Simpson, S. L.; Jarolimek, C. V.; Jolley, D. F. Diffusive gradients in thin films technique provide robust prediction of metal bioavailability and toxicity in estuarine sediments. *Environ. Sci. Technol.* **2014**, *48* (8), 4485−4494.

(31) Posthuma, L.; Traas, T. P.; Suter, G. General introduction to species sensitivity distributions. *Species Sensitivity Distrib. Ecotoxicol.* **2002**, 3−10.

(32) Fox, D. R.; van Dam, R. A.; Fisher, R.; Batley, G. E.; Tillmanns, A. R.; Thorley, J.; Schwarz, C. J.; Spry, D. J.; McTavish, K. Recent developments in species sensitivity distribution modeling. *Environ. Toxicol. Chem.* **2020**, *40* (2), 293−308.

https://doi.org/10.1021/acsestwater.5c00307
ACS EST Water 2025, 5, 5145−5156

(33) Gu, Y. G.; Gao, Y. P.; Huang, H. H.; Wu, F. X. First attempt to assess ecotoxicological risk of fifteen rare earth elements and their mixtures in sediments with diffusive gradients in thin films. *Water Res.* **2020**, *185*, No. 116254.
(34) US EPA. *Species Sensitivity Distribution (SSD) Toolbox: What is the SSD Toolbox?* https://www.epa.gov/comptox-tools/species-sensitivity-distribution-ssd-toolbox. (accessed 2025−07−30).
(35) Fang, T.; Yang, K.; Wang, H.; Fang, H. Y.; Liang, Y. Y.; Zhao, X. X.; Gao, N.; Li, J.; Lu, W. X.; Cui, K. Trace metals in sediment from Chaohu Lake in China: Bioavailability and probabilistic risk assessment. *Science of The Total Environment* **2022**, *849*, No. 157862.
(36) Li, H. S.; Gu, Y. G.; Liang, R. Z.; Wang, Y. S.; Jordan, R. W.; Wang, L. G.; Jiang, S. J. Heavy metals in riverine/estuarine sediments from an aquaculture wetland in metropolitan areas, China: Characterization, bioavailability and probabilistic ecological risk. *Environ. Pollut.* **2023**, *324*, No. 121370.
(37) Gu, Y. G.; Gao, Y. P.; Jiang, S. J.; Jordan, R. W.; Yang, Y. F. Ecotoxicological risk of antibiotics and their mixtures to aquatic biota with the DGT technique in sediments. *Ecotoxicology* **2023**, *32* (4), 536−543.
(38) Gu, Y. G.; Wang, Y. S.; Jordan, R. W.; Su, H.; Jiang, S. J. Probabilistic ecotoxicological risk assessment of heavy metal and rare earth element mixtures in aquatic biota using the DGT technique in coastal sediments. *Chemosphere* **2023**, *329*, No. 138592.
(39) Gu, Y. G.; Huang, H. H.; Gong, X. Y.; Liao, X. L.; Dai, M.; Yang, Y. F. Application of diffusive gradients in thin films to determine rare earth elements in surface sediments of Daya Bay, China: Occurrence, distribution and ecotoxicological risks. *Mar. Pollut. Bull.* **2022**, *181*, No. 113891.
(40) Wang, F.; Li, X. G.; Tang, X. H.; Sun, X. X.; Zhang, J. L.; Yang, D. Z.; Xu, L. J.; Zhang, H.; Yuan, H. M.; Wang, Y. T.; Yao, Y. L.; Wang, C. Z.; Guo, Y.; Ren, Q. P.; Li, Y. L.; Zhang, R. W.; Wang, X.; Zhang, B.; Sha, Z. L. The seas around China in a warming climate. *Nature Reviews Earth & Environment* **2023**, *4* (8), 535−551.
(41) Liu, H.; Zhao, B.; Jin, M.; Wang, R.; Ding, Z. R.; Wang, X.; Xu, W. J.; Chen, Q. H.; Tao, R. Z.; Fu, J. P.; Xie, D. P. Anthropogenic-induced ecological risks on marine ecosystems indicated by characterizing emerging pollutants in Pearl River Estuary. *China. Science of The Total Environment* **2024**, *926*, No. 172030.
(42) Wang, Y. S.; Wu, F. X.; Gu, Y. G.; Huang, H. H.; Gong, X. Y.; Liao, X. L. Polycyclic aromatic hydrocarbons (PAHs) in the intertidal sediments of Pearl River Estuary: Characterization, source diagnostics, and ecological risk assessment. *Mar. Pollut. Bull.* **2021**, *173*, No. 113140.
(43) Sheng, C.; Jiao, J. J.; Luo, X.; Zuo, J. C.; Jia, L.; Cao, J. H. Offshore freshened groundwater in the Pearl River estuary and shelf as a significant water resource. *Nat. Commun.* **2023**, *14* (1), 3781.
(44) Gu, Y. G. Risk assessment of eight metals and their mixtures to aquatic biota in sediments with diffusive gradients in thin films (DGT): a case study in Pearl River intertidal zone. *Environmental Sciences Europe* **2021**, *33* (1), 122.
(45) Ji, X. M.; Sheng, J. Y.; Tang, L. Q.; Liu, D. B.; Yang, X. L. Process study of circulation in the Pearl River Estuary and adjacent coastal waters in the wet season using a triply-nested circulation model. *Ocean Modelling* **2011**, *38* (1), 138−160.
(46) Brady, J. P.; Kinaev, I.; Goonetilleke, A.; Ayoko, G. A. Comparison of partial extraction reagents for assessing potential bioavailability of heavy metals in sediments. *Mar. Pollut. Bull.* **2016**, *106* (1), 329−334.
(47) Müller, G. Index of geoaccumulation in sediments of the Rhine River. *Geojournal* **1969**, *2* (3), 108−118.
(48) CEMS (China Environmental Monitoring Station) *Natural background values of soil elements in China*. In China Environmental Science Press: 1990; pp 418−450.
(49) Zhang, G.; Cheng, W. C.; Chen, L. H.; Zhang, H.; Gong, W. P. Transport of riverine sediment from different outlets in the Pearl River Estuary during the wet season. *Marine Geology* **2019**, *415*, 105957.
(50) Fang, Z. M.; Wang, W. X. Dynamics of trace metals with different size species in the Pearl River Estuary, Southern China. *Science of The Total Environment* **2022**, *807*, No. 150712.
(51) Wang, S. S.; Cao, Z. M.; Lan, D. Z.; Zheng, Z. C. Geochemical characteristics of sediment of Pearl River Estuary and its paleoenvironmental evolution. *Earth Sci.* **2010**, *35* (2), 261−267.
(52) Tomlinson, D.; Wilson, J.; Harris, C.; Jeffrey, D. Problems in the assessment of heavy-metal levels in estuaries and the formation of a pollution index. *Helgoländer meeresuntersuchungen* **1980**, *33*, 566−575.
(53) Gu, Y. G.; Jiang, S. J.; Jordan, R. W.; Huang, H. H.; Wu, F. X. Nonmetric multidimensional scaling and probabilistic ecological risk assessment of trace metals in surface sediments of Daya Bay (China) using diffusive gradients in thin films. *Science of The Total Environment* **2023**, *867*, No. 161433.
(54) Gu, Y. G.; Gao, Y. P. An unconstrained ordination- and GIS-based approach for identifying anthropogenic sources of heavy metal pollution in marine sediments. *Mar. Pollut. Bull.* **2019**, *146*, 100−105.
(55) Gu, Y. G.; Ke, C. L.; Gao, Y. P.; Liu, Q.; Li, Y. F. Nonmetric multidimensional scaling and adverse effects on aquatic biota of polycyclic aromatic hydrocarbons in sediments: A case study of a typical aquaculture wetland. *China. Environmental Research* **2020**, *182*, No. 109119.
(56) Gao, Y. P.; Geng, M. Z.; Wang, G. Y.; Yu, H.; Ji, Y. M.; Jordan, R. W.; Jiang, S. J.; Gu, Y. G.; An, T. C. Environmental and dietary exposure to 24 polycyclic aromatic hydrocarbons in a typical Chinese coking plant. *Environ. Pollut.* **2024**, *346*, No. 123684.
(57) Liang, R. Z.; Gu, Y. G.; Li, H. S.; Han, Y. J.; Niu, J.; Su, H.; Jordan, R. W.; Man, X. T.; Jiang, S. J. Multi-index assessment of heavy metal contamination in surface sediments of the Pearl River estuary intertidal zone. *Mar. Pollut. Bull.* **2023**, *186*, No. 114445.
(58) Grew, E. S. Mineralogy, petrology and geochemistry of beryllium: An introduction and list of beryllium minerals. *Reviews in Mineralogy and Geochemistry* **2002**, *50* (1), 1−76.
(59) Åström, M. E.; Yu, C.; Peltola, P.; Reynolds, J. K.; Österholm, P.; Nystrand, M. I.; Augustsson, A.; Virtasalo, J. J.; Nordmyr, L.; Ojala, A. E. K. Sources, transport and sinks of beryllium in a coastal landscape affected by acidic soils. *Geochim. Cosmochim. Acta* **2018**, *232*, 288−302.
(60) Cánovas, C. R.; Basallote, M. D.; Macías, F.; Olías, M.; Pérez-López, R.; Nieto, J. M. Thallium in environmental compartments affected by acid mine drainage (AMD) from the Iberian Pyrite Belt (IPB): From rocks to the ocean. *Earth-Science Reviews* **2022**, *235*, No. 104264.
(61) Marafatto, F. F.; Dähn, R.; Grolimund, D.; Göttlicher, J.; Voegelin, A. Thallium sorption by soil manganese oxides: Insights from synchrotron X-ray micro-analyses on a naturally thallium-rich soil. *Geochim. Cosmochim. Acta* **2021**, *302*, 193−208.
(62) Cruz-Hernández, Y.; Ruiz-García, M.; Villalobos, M.; Romero, F. M.; Meza-Figueroa, D.; Garrido, F.; Hernández-Alvarez, E.; Pi-Puig, T. Fractionation and mobility of thallium in areas impacted by mining-metallurgical activities: Identification of a water-soluble Tl(I) fraction. *Environ. Pollut.* **2018**, *237*, 154−165.
(63) Du, Y. P.; Shi, L. F.; Cao, X. Y.; Zhao, F. Q.; Hu, P. J.; Ying, R. R.; Gu, S. Y.; Wu, L. H.; Luo, Y. M.; Christie, P. Potential high-risk release sources of thallium and arsenic from surrounding rocks of a typical thallium and arsenic mining area in southwest China. *Science of The Total Environment* **2024**, *935*, No. 173371.
(64) Gill, W. A.; Alhokbany, N.; Janjua, M. R. S. A. Adsorption of molecular hydrogen on Be_3 Al $_2(SiO_3)_6$-beryl: theoretical insights for catalysis, hydrogen storage, gas separation, sensing, and environmental applications. *RSC Adv.* **2024**, *14* (6), 3782−3789.
(65) Huang, Y.; Wang, D. X.; Jiang, J. H.; Gong, J.; Liu, Y. X.; Li, L.; Kong, L. J.; Ruan, Y.; Lv, H.; Chen, Y. H.; Chen, Z. B.; Liang, Q.; Chen, D. Y. Release and mobility characteristics of thallium from polluted farmland in varying fertilization: Role of cation exchange. *Journal of Hazardous Materials* **2023**, *458*, No. 131928.
(66) Liu, Y.; Wei, L. Z.; Luo, D. G.; Xiao, T. F.; Lekhov, A.; Xie, X.; Huang, X. X.; Su, X. T. Geochemical distribution and speciation of

https://doi.org/10.1021/acsestwater.5c00307
ACS EST Water 2025, 5, 5145−5156

thallium in groundwater impacted by acid mine drainage (Southern China). *Chemosphere* **2021**, *280*, No. 130743.
(67) Kam, O. R.; Bakouan, C.; Zongo, I.; Guel, B. Removal of thallium from aqueous solutions by adsorption onto alumina nanoparticles. *Processes* **2022**, *10* (9), 1826.
(68) Long, E. R. Calculation and uses of mean sediment quality guideline quotients: A Critical Review. *Environ. Sci. Technol.* **2006**, *40* (6), 1726−1736.
(69) Long, E. R.; MacDonald, D. D.; Severn, C. G.; Hong, C. B. Classifying probabilities of acute toxicity in marine sediments with empirically derived sediment quality guidelines. *Environ. Toxicol. Chem.* **2000**, *19* (10), 2598−2601.

https://doi.org/10.1021/acsestwater.5c00307
ACS EST Water 2025, 5, 5145−5156